ELSEVIER

Journal of Nuclear Materials 266–269 (1999) 37–43

journal of nuclear materials

Volume recombination and detachment in JET divertor plasmas

G.M. McCracken [a,*], R.D. Monk, A. Meigs, L. Horton, L.C. Ingesson, J. Lingertat, G.F. Matthews, M.G. O'Mullane, R. Prentice, M.F. Stamp, P.C. Stangeby [b]

[a] *JET Joint Undertaking, Abingdon OX14 3EA, UK*
[b] *University of Toronto, Institute for Aerospace Studies, Toronto, Canada M3H 5T6*

Abstract

The spatial distribution of recombination has been studied in the detaching phases of L and H-mode discharges. Recombination is detected by the sudden increase in intensity of the high quantum number states of the Balmer series of hydrogen. In L-mode, detachment occurs completely and the radiation moves to a region near the X-point. In H-mode, detachment only occurs between ELMs. There is a marked decrease in the pedestal T_e inside the separatrix and loss of confinement before detachment takes place.

Keywords: Radiation; JET; Tokamak; Detachment; Divertor

1. Introduction

Volume recombination in hydrogenic plasmas has recently been shown, both experimentally and theoretically, to play an important role in plasma detachment from the target plates of diverted discharges [1,2]. Experimental evidence of recombination has been obtained in JET from the increase in the ratio of the intensities of the Balmer series lines of excited hydrogen atoms, D_γ/D_α and D_δ/D_α [3]. The start of recombination is closely correlated, both spatially and temporally, with the onset of detachment. Detachment is generally defined here as when the ion current to the target, as determined by the Langmuir probes, does not increase with $\bar{n}_e^2$ as expected [4]. Recombination enhances hydrogenic radiation and reduces the power flow to the target. It is also a clear indicator of very low plasma temperature, $\sim$1 eV.

In the present paper we have examined the spatial distribution of recombination in detail using a CCD camera with optical filters at the D_γ and D_α lines of the hydrogen Balmer series and have extended our discussion to H-mode discharges. In ohmic and L-mode discharges with a density ramp, recombination occurs first at the inner target and then, near the density limit, it occurs at the outer target. At the outer target the D_γ/D_α and D_δ/D_α ratios have been measured as a function of radial position. It is shown that in both L-mode and H-mode discharges recombination predominantly takes place close to the separatrix strike point.

2. Diagnostics

Spectroscopically resolved data in the visible are available from integrated views of both the inner and outer JET divertor targets, measured simultaneously. Two spectrometers (KS3) are survey instruments and routinely monitor the deuterium Balmer series lines D_α, (656.27 nm), D_β, (486.13 nm) and D_γ (434.05 nm). A second pair of spectrometers (KT3A/B) have 12 spatial tracks across the outer target, each 13 mm wide. One (KT3B) covers the visible spectrum range, 400–700 nm, with a resolution of 0.1 nm and can monitor D_β, D_γ and

* Corresponding author. Tel.: +44 1235 46 5063; fax: +44 1235 46 4535; e-mail: garry.mcracken@jet.uk.

0022-3115/99/$ – see front matter
PII: S0022-3115(98)00571-6

D_δ (410.17 nm) simultaneously. The second (KT3A) also covers the near UV (200–700 nm) with a resolution of 0.05 nm. KT3A has been used to measure the electron density using the Stark broadening of the high n states of the deuterium Balmer lines [5]. The spatial distribution across the inner and outer target of different spectroscopic lines is obtained, with 3 mm resolution at the target, from three CCD cameras with interference filters, (KL2). Optical filters have been used to study the D_α and the D_γ lines, as well as the CII line at 657.8 nm, which allows us to look at the spatial distribution of the D_γ/D_α ratio in much more detail than in our earlier studies [4]. In addition to the spectroscopic diagnostics there is a poloidal array of 40 fixed Langmuir probes in the inner and outer targets which are used to measure local ion saturation current and electron temperature. An interferometer KG6D is used to measure the line integral density across the outside divertor target fan just above the target. The lines of sight of these diagnostics are shown in Fig. 1.

In addition to the above diagnostics there are three cameras with optical filters looking at D_α, D_γ and CII (658 nm) tangentially into the torus via an endoscope. At present the data is recorded on videotape and is uncalibrated but it allows the vertical height of the D_γ and D_α radiation to be assessed.

3. Results

3.1. Ohmic and L-mode discharges

Ohmic and L-mode discharges, with density ramps obtained by gas puffing, have been studied routinely to assess the density limit under a range of different conditions [6]. The general behaviour of an L-mode discharge with 2 MW of neutral beam heating and with the strike point on the horizontal target (see Fig. 1) is shown in Fig. 2. As the density rises, first the inner target detaches and then, near the density limit, the outer target detaches. Detachment is first observed through the drop in the ion current to the targets, Fig. 2(d). This is more clear cut in the case of the outer target than the inner one. There is a discontinuity in the density when the plasma detaches from the outer target and the fuelling efficiency changes, Fig. 2(a). This behaviour seems to be characteristic of tokamaks with closed divertors [7]. The D_γ/D_α ratio, Fig. 2(b), measured with the visible spectrometer (KS3) viewing the inner and outer targets separately, at first decreases as the density rises, as is expected from the atomic physics rate coefficients characteristic of excitation only [8,9], and reaches approximately the same value, $D_\gamma/D_\alpha \sim 0.013$, in each case just before detachment. This corresponds to an average density of $\sim 1 \times 10^{20}$ m^{-3} [9]. The line integral density measured with the interferometer at the outer target is shown in Fig. 2(c). At the time of outer target detach-

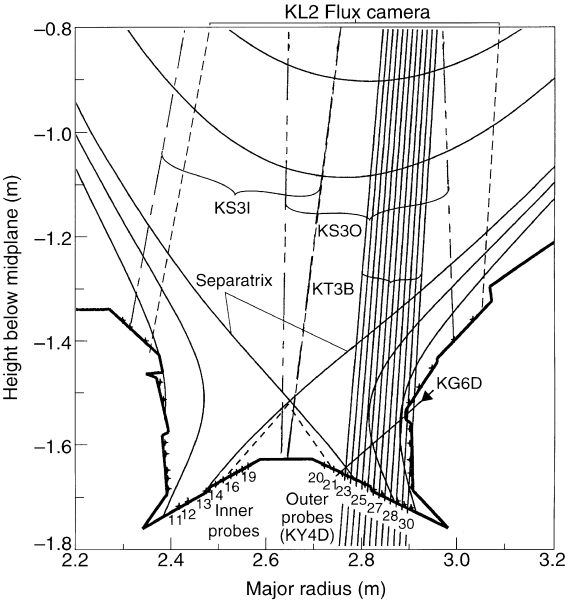

Fig. 1. Poloidal cross section of JET showing the lines of sight of the spectroscopic diagnostics, the probes and the divertor interferometer.

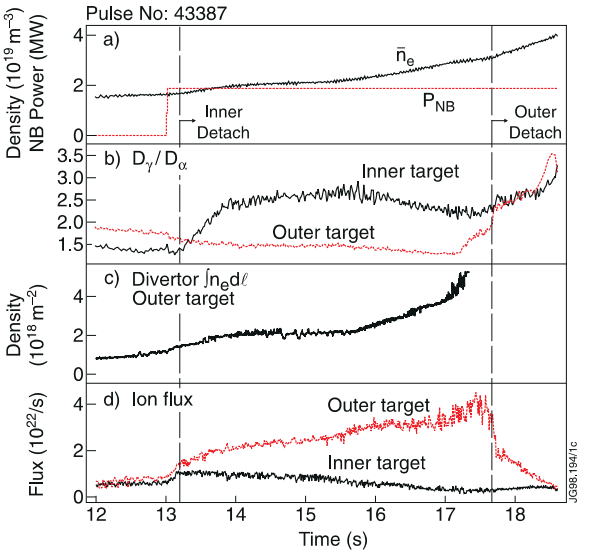

Fig. 2. Time evolution of the parameters of an L-mode discharge during a density ramp with strike points on the horizontal target. #43887. (a) Core density $\bar{n}_e$ and neutral beam power P_{NB}. (b) Ratio of the integrated D_γ and D_α intensities at the inner and outer targets. (c) Line integral density at the outer target. (d) Integrated ion current to the inner and outer targets.

ment it is $>5 \times 10^{18}$ m^{-2}, corresponding to a maximum density of $\sim 8 \times 10^{19}$ m^{-3}. The interferometer stops working at an integral density of $\sim 5 \times 10^{18}$ m^{-2} due to refraction of the microwaves.

Coincident with the drop in ion current there is a large rise in the absolute level of the D_γ and D_α line intensity and an increase in the D_γ/D_α ratio as shown in Fig. 2(b). The abrupt increase in the D_γ/D_α ratio is characteristic of the onset of recombination [4,10]. Discharges in hydrogen required higher power to reach the L–H mode transition which allowed L-mode discharges to be studied at input powers of 4 and 6 MW. However, the value of the D_γ/D_α ratio reached just prior to detachment was the same for these discharges, indicating that plasma conditions were very similar. The electron temperature measured at the probes in the outer target falls to <5 eV just before detachment as discussed in detail previously [4].

The strike points can be moved from the horizontal target (illustrated in Fig. 1) to the vertical target. In this configuration detachment, as measured by the ion saturation current, and recombination, as measured by the D_γ/D_α ratio, both change much more gradually, Fig. 3. The detachment at the inner target takes place at higher density and the detachment of inner and outer target occur almost simultaneously. There is a further abrupt reduction in the ion current and change of slope of $\bar{n}_e$, corresponding to MARFE formation, at 19.8 s. Similar

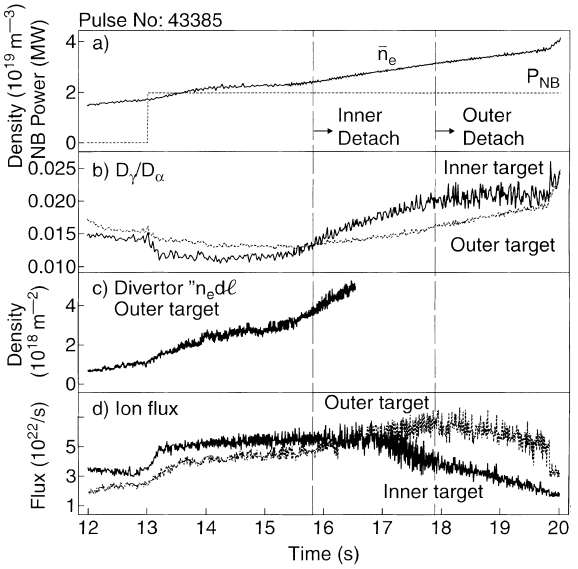

Fig. 3. Time evolution of the parameters of an L-mode discharge during a density ramp with strike points on the vertical target. #43885. (a) Core density $\bar{n}_e$ and neutral beam power P_{NB}. (b) Ratio of the integrated D_γ and D_α intensities at the inner and outer targets. (c) Line integral density at the outer target. (d) Integrated ion current to the inner and outer targets.

densities, as measured by the interferometer at the outer target, are required to induce detachment both with the strike point on the horizontal and vertical targets and the value of the D_γ/D_α ratio at detachment is the same. The interferometer chord still goes through the SOL in the divertor with the strike point on the vertical target, although the width of the SOL along the line of sight is smaller.

The position of the recombination is observed from the D_γ/D_α ratio measured with the cameras as shown in Fig. 4. Because of the finite bandwidth of the filter (10 nm), care must be taken that the D_γ signal is not contaminated with impurity lines or the CD band at 431 nm, both of which tend to occur at low densities. However, by cross-checking with spectrometer data, despite their poorer spatial resolution, the conditions under which the D_γ/D_α ratio increases can be ascertained. The contour plots of Fig. 4 show that the D_α intensity is highest at the inner target and is centred near the inner strike point. The intensity increases as the density rises up to 16.8 s. During most of this time the ratio of D_γ/D_α is constant but moves gradually to larger major radius, i.e. closer to the X-point, see Fig. 1. The tangential camera view shows that the region of most intense radiation is moving vertically up towards the X-point. Between 16.0 and 17.5 s the D_γ/D_α ratio at the strike point decreases. This seems unlikely to be due to less recombination. A more probable explanation is that the temperature at the inner target is dropping further. This results in a reduced value of the D_γ/D_α ratio [8,11]. When detachment occurs at the outer target, as indicated by the increase in the D_γ/D_α ratio and the discontinuity in the density, the peak D_γ/D_α ratio jumps to a position between $R = 2.60$ and 2.68 m Fig. 4. The rise in the D_γ/D_α ratio at the "outer" target as seen in Fig. 2, actually corresponds to radiation from near the X-point. No accurate measure of the vertical height of this radiation is available at present but the radial position is similar to that of the total radiation, obtained from a tomographic reconstruction of the bolometer array data.

3.2. H-mode discharges

When higher power neutral beam heating is turned on ($\geqslant 3$ MW in deuterium) there is a rapid transition from L-mode to H-mode with the onset of ELMs and the formation of a temperature pedestal just inside the separatrix [12]. If there is no additional gas puffing the inner target plasma remains detached and the outer target plasma is attached. In H-mode with modest gas puffing ($\leqslant 10^{22}$ D/s) recombination is observed at the inner target.

Gas puffing has been increased in steps in successive discharges but has little effect on the density. The fuelling efficiency decreases and the density remains approximately constant [13,14]. A discharge with high gas

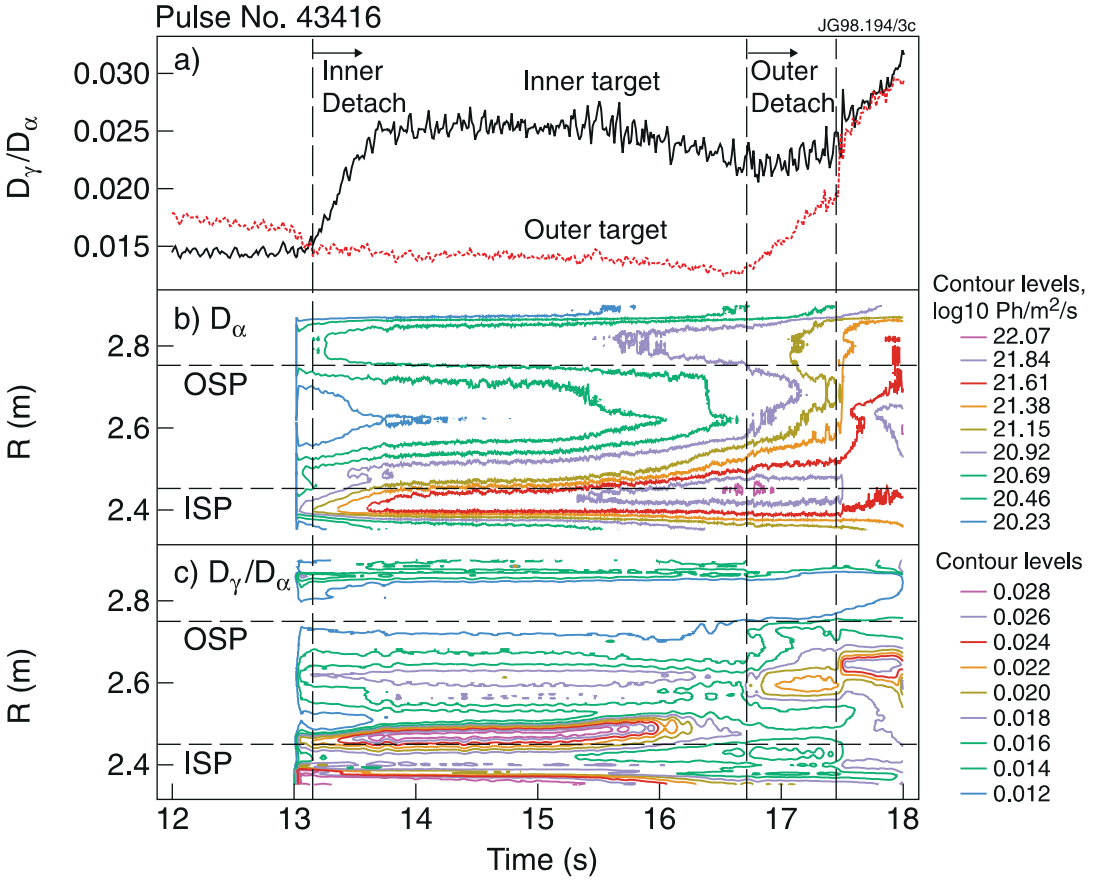

Fig. 4. Time and space development of the D_α intensity and the D_γ/D_α intensity ratio in an L-mode discharge with 2 MW neutral beam heating and a density ramp induced by gas puffing. The inner (ISP) and outer (OSP) strike points are indicated. Shot #43416, $I_p = 2.0$ MA, $B_t = 2.5$ T. (a) Ratio of the integrated D_γ and D_α intensities at the inner and outer targets. (b) Contours of D_α intensity. (c) Contours of D_γ/D_α intensity ratio.

puffing (3×10^{22} D/s) is shown in Fig. 5. The increase in gas puffing causes the radiated power to increase and the energy confinement time to decrease. The H89 factor falls from ~1.8 to 1.5, Fig. 5, as T_e, measured by the ECE heterodyne radiometer at the pedestal ($r/a = 0.9$), drops from 1.0 to 0.4 keV. At 18 s, after the gas puff has been on for about 1 s, the D_γ/D_α ratio, as observed with the spectrometer looking at the two spatial integrals of the inner and outer targets, shows an upward jump at the outer target and and there is a corresponding drop in the integral ion current to the outer target. Other features of this transition are a sudden increase in the power radiated to 50–60% of the nominal input power and a change in the character of the ELMs from type I to type III. The electron temperature T_e, measured by the probes in the target near the strike point, falls to <3 eV, Fig. 5(h). There is further drop in H89. In some cases it falls back to the L-mode level as measured in the same discharge in a phase with lower neutral beam heating. These features are all characteristic of plasma detachment from the outer target. At this stage since the ELMs are small, with a frequency ~100 Hz, and the H89 factor is less than 1.5 it is a rather poor quality H-mode. When the gas puff is turned off at 21.8 s the plasma reattaches at the outer target and the H89 factor begins to rise again. Similar discharges with slightly less gas puffing ($<3 \times 10^{22}$ D/s) can result in a reduction in the pedestal T_e, and a deterioration in confinement without leading to detachment provided T_e at the target, between ELMs, does not fall below ~5 eV. The ion current to the outer target does not drop. The size of gas puff required to induce detachment does not seem to be strongly dependent on the input power in the 8–14 MW range.

During the detached phase there are large spikes in the ion current to the target and in the plasma temperature, measured by the target probes, which are coincident with the ELM spikes observed on the D_α signal, Fig. 5(f), (g) and (h). A triple probe with a time response of 0.1 ms was used. From the triple probe data the plasma is observed to reattach briefly during the ELMs;

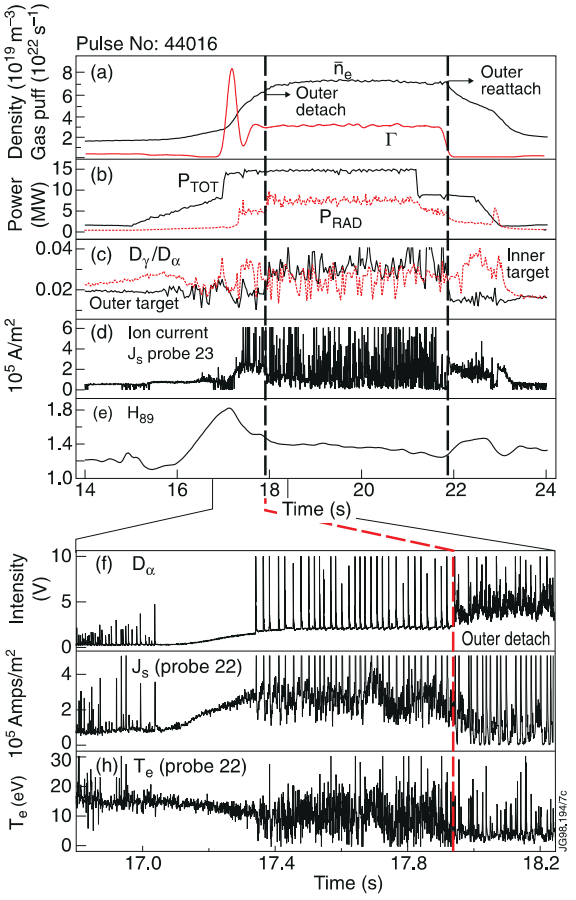

Fig. 5. Time evolution of the parameters of an ELMy H-mode discharge during strong gas puffing #44016. (a) Core density $\bar{n}_e$ and deuterium gas puff rate Γ. (b) Total input power, P_{tot}, and total radiated power, P_{rad}. (c) Ratio of the integrated D_γ and D_α intensities at the inner and outer targets. (d) Saturated ion current density at probe 23 near the strike point on the outer target. (e) Scaled energy confinement time H89. (f) D_α intensity at the outer divertor on expanded time scale showing transition from Type I to type III ELMs. (g) Ion current to triple probe 22, on expanded scale, showing drop in current when outer target detaches at 17.93 s. (h) T_e from triple probe 22, showing drop in temperature when outer target detaches at 17.93 s.

the D_γ and D_α spectroscopic signals are too slow to resolve the effects of the ELM. Less data is available for H-mode discharges with the strike point on the vertical target, but unlike the L-mode there are no obvious differences in the detachment behaviour between horizontal and vertical targets.

The spatial distribution of recombination is much more difficult to determine in H-mode than in L-mode. Recombination can be observed at the inner target during the L-mode phase which preceeds the H-mode condition. When the H-mode develops, the maxima in the D_α, D_γ and CII radiation come from near the strike points. The D_α and D_γ intensities are about 3 times higher at the inner strike point than the outer but the signals are unfortunately partly saturated during the high gas puffing phase from 17.2 to 20.7 s. Data from the camera with the D_γ filter is difficult to interpret in the presence of the ELMs.

The spatial distribution of the higher n Balmer series have been measured with the KT3A and KT3B visible spectrometers over the range $R = 2.74$–2.9 m during the detached phase of the high power discharges. The spatial distribution of the intensity of these states is compared to the intensity of the D_α and to a tomographic reconstruction of the total radiation from bolometers in Fig. 6. It is seen that, after detachment, while most of the total radiation comes from the outer target near the strike point, the maximum in the D_α radiation still comes from the inner target. This is different from discharges with impurity puffing which result in MARFE formation and radiation from near the X-point [15]. Radiation from the transitions $n = 5 \rightarrow 2$, $n = 6 \rightarrow 2$, $n = 9 \rightarrow 2$, $n = 10 \rightarrow 2$, and $n = 11 \rightarrow 2$ are observed at the outer target. The fact that these lines are observable

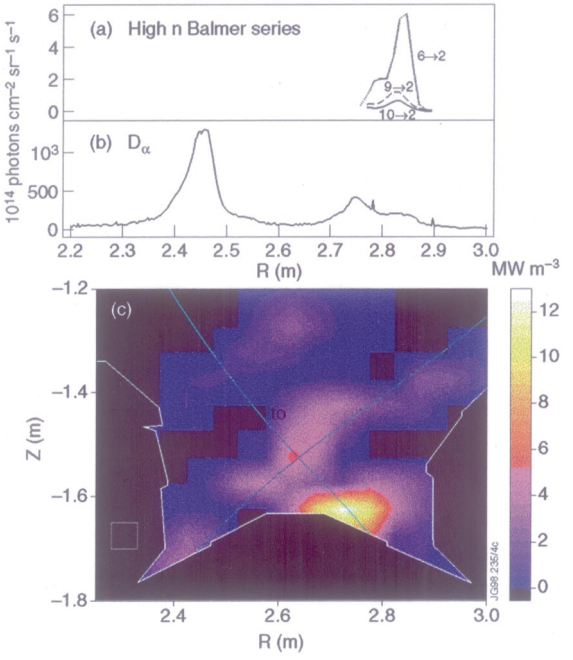

Fig. 6. Spatial distribution of total radiation and deuterium radiation in a neutral beam heated discharge, detached at the outer target, #44016. $I_p = 2.6$ MA, $B_t = 2.7$ T, $P_{tot} = 14.6$ MW, $n_e = 7.3 \times 10^{19}$ m^{-3}. Gas puff 3.1×10^{22} D/s. (a) Intensity of the Balmer series transitions $n = 6 \rightarrow 2$, $n = 9 \rightarrow 2$ and $n = 10 \rightarrow 2$, at the outer target, measured with the visible spectrometers, KT3A/B (line integrated). (b) D_α intensity from the flux camera, KL2 (line integrated). (c) Tomographic reconstruction of the total radiation from bolometer array.

indicates that some recombination is taking place. The high n lines also allow the density along a line of sight to be calculated from the Stark broadening [16]. Densities in the range $n_e = 3–5 \times 10^{20}$ m^{-3} are obtained with very similar results from the analysis of $n = 9 \rightarrow 2$, $n = 10 \rightarrow 2$, and $n = 11 \rightarrow 2$ transitions [5].

The photon emissivity distribution of the various transitions from principal quantum number $n = 3 \rightarrow 2$ to $n = 11 \rightarrow 2$ at major radii, $R = 2.80$ and 2.84 m during the detached phase of a H-mode discharge with high gas puffing is shown in Fig. 7. These data have been compared with calculations of the photon emissivity coefficients (PECs) calculated using the ADAS atomic data and a radiative-collisional model [11]. The experimental PECs have been obtained from the data by dividing the line intensity by the local n_e^2, measured by the Stark broadening of the high n transitions. There is good agreement between the measured PECs and those calculated for recombination. The absolute values agree with the assumption of a local $T_e = 0.7–1.0$ eV and an assumed line integral length of the emitting region of 0.03 m.

4. Discussion

Detachment and recombination occur when the plasma temperature at the target falls below ~5 eV, as measured by the probes. The radiation moves upwards and increases, causing T_e to drop further and recombination to be enhanced. In the case of ohmic and L-mode discharges, further fuelling causes increased density which results in an instability. More power is then radiated than is being applied and the plasma disrupts. In the steady state ELMy H-mode this seldom happens. Increased fuelling has little effect on the density; the fuelling efficiency simply decreases. Thus the detached mode appears to be stable with 50–60% of the total input power being radiated.

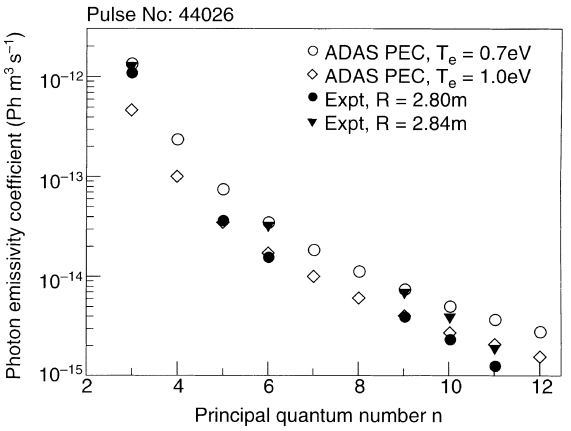

Fig. 7. Population distribution of the principal quantum states of deuterium at two major radii, $R = 2.80$ and 2.84 m in a neutral beam heated discharge detached at the outer target by gas puffing. #44026. $I_p = 2.6$ MA, $B_t = 2.7$ T, $P_{tot} = 9.2$ MW, $n_e = 7.5 \times 10^{19}$ m^{-3}. Gas puff $= 3.7 \times 10^{22}$ D/s. The experimental data has been compared to the photon emissivity calculated from ADAS [11] by dividing by the density measured by Stark broadening (4×10^{20} m^{-3}) and an assumed radiating depth of 0.03 m.

It is important to know whether detachment is playing a role in the reduction of confinement. In the H-mode case the effect of gas puffing is to increase the total radiation and to reduce the local edge temperature in the pedestal. The lowered pedestal T_e reduces the confinement well before there is any indication of detachment or recombination at the outer target, Fig. 5(a). With continued gas puffing the density at the target continues to rise and T_e falls until the conditions for detachment and recombination occur, Fig. 5(b). They then occur simultaneously within the time resolution of the spectroscopic diagnostics, ~50 ms. At this point the character of the ELMs changes from type I to type III. When the gas puffing stops the confinement starts to recover; it does not fully return to the initial H-mode value in Fig. 5 only because the beam heating power has been reduced at that stage. The spatial distribution of the recombination is much more difficult to determine in H-mode than in L-mode. In the discharge in Fig. 5 the discharge is in L-mode before 16 s and the recombination signal is seen at the inner strike point as in other L-mode discharges. When the transition to H-mode occurs the D_α and D_γ radiation still are predominantly at the inner target and there is no obvious indication of recombination from the ratio of the D_α and D_γ signals measured with the flux camera. When the outer target detaches, high n states indicating recombination are observed at the outer target with the KT3A/KT3B spectrometers.

The comparison between the approach to detachment with horizontal and vertical targets is interesting. In the JET Mk I divertor there was little difference between the density required for detachment at the inner and outer targets. In Mk II however, detachment occured at ~30% lower density than in MkI [6] and, as seen from Figs. 2 and 3, there is a marked difference between detachment on the horizontal and vertical targets. Using the horizontal target, detachment occurs at much lower $\bar{n}_e$ on the inner target than on the outer, while using the vertical target detachment occurs at the inner and outer targets at roughly the same density. The approach to detachment is also rather gradual on the vertical target while on the horizontal one it is quite abrupt. The geometry of the SOL is well known to be different in the two cases, with the recycling neutrals entering the SOL near the hot, dense plasma at the separatrix with the vertical target and going into the low

density outer SOL with the horizontal target. This results in quite a different recycling pattern in the two cases. The more symmetric behaviour with vertical targets is possibly caused by the private flux zone being common to the inner and outer separatrices. If it is assumed that the SOL is reasonably transparent to recycling neutrals then the density will build up in the private flux zone (PFZ) between the strike points and the neutral source will be the same for inner and outer separatrices. With the horizontal target the recycling neutrals are separated by the "divertor legs" and the PFZ. It is thus probable that the difference in the recycling pattern leads to the difference in the detachment behaviour.

5. Conclusions

The onset of recombination coincides with detachment in JET, at both inner and outer divertor targets. The recombination is concentrated around the strike point in both cases. This means that the plasma temperature must locally be <1 eV. After detachment occurs the radiation moves upwards and there is some evidence for recombination occurring at the X-point in L-mode discharges. There is no evidence that this occurs in H-mode conditions.

The observation of recombination is a valuable diagnostic which confirms the results from the probes that detachment is more gradual and more symmetric when the strike points are on the vertical targets. When the strike point is on the horizontal targets detachment occurs at lower density on the inner target than at the outer target.

Detachment observed with the probes, the rise in D_γ/D_α ratio and the movement of the radiation distribution, all occur during H-mode discharges when a sufficiently high gas injection is applied. However the initial effect of the gas is to reduce T_e inside the separatrix at the profile pedestal. This has the consequence of reducing the energy confinement, H89 falling from $\sim$2.0 to <1.5, ie no longer being in good H-mode, despite the high power input. With continued gas puffing the outer target detaches. It thus appears that it is not possible to have detached discharges with good H-mode confinement. This is an important conclusion in that the power to the target cannot be spatially dissipated by radiation in the way it can be in ohmic or L-mode plasmas.

References

[1] D. Lumma, J.L. Terry, B. Lipschultz, Phys. Plasmas 4 (1997) 2555.
[2] S.I. Krasheninnikov, Phys. Plasmas 4 (1997) 1638.
[3] A. Loarte, J. Nucl. Mat. 241–243 (1997) 118.
[4] G.M. McCracken, M.F. Stamp, R.D. Monk et al., Nuclear Fusion, 38 (1998) 619.
[5] A.G. Meigs, to be published in Proc. 25th Eur. Conf. on Controlled Fusion and Plasma Physics, Prague, 1998.
[6] R.D. Monk et al., in: Proc. 24th Eur. Conf. on Controlled Fusion and Plasma Physics, Berchtesgaden, vol. 21A, Pt. I, European Physical Society, Geneva, 1997, p. 117.
[7] G.M. McCracken, B. Lipschultz, B. Labombard et al., Phys. Plasmas 4 (1997) 1681.
[8] L.C. Johnson, E. Hinnov, J. Quant. Spectr. Rad. Transf. 13 (1973) 33.
[9] T. Fujimoto, S. Miyachi, K. Sawada, Nuclear Fusion 28 (1988) 1255.
[10] J.L. Terry, B. Lipschultz, D. Lumma et al., in: Proc. 24th Eur. Conf. on Controlled Fusion and Plasma Physics, Berchtesgaden, vol. 21A, Pt. II, European Physical Society, Geneva, 1997, p. 573.
[11] H.P. Summers, Atomic Data and Analysis Structure Users Manual, JET Report IR(94) 06, JET Joint Undertaking, Abingdon, UK, 1994.
[12] M. Keilhacker for the JET team, Plasma Phys. and Contr. Fusion 39 (Suppl. 12B) (1997) B1.
[13] G. Saibene, B. Balet, S. Clement et al., in: Proc. 24th Eur. Conf. on Controlled Fusion and Plasma Physics, Berchtesgaden, vol. 21A, Pt. I, European Physical Society, Geneva, 1997, p. 49.
[14] G.F. Matthews, P. Andrew, B. Balet et al., these Proceedings.
[15] G.F. Matthews, B. Balet, J.G. Cordey et al., Nuclear Fusion, 39 (1) (1999), to be published.
[16] B.L. Welch, H.R. Griem, J.L. Terry et al., Phys. Plasmas 2 (1995) 4246.